Green Chemistry

Cite this: *Green Chem.*, 2012, **14**, 1515

www.rsc.org/greenchem

PAPER

A one-pot hydrothermal synthesis of sulfur and nitrogen doped carbon aerogels with enhanced electrocatalytic activity in the oxygen reduction reaction†

Stephanie-Angelika Wohlgemuth,*[a] Robin Jeremy White,[a] Marc-Georg Willinger,[b] Maria-Magdalena Titirici[a] and Markus Antonietti[a]

Received 1st March 2012, Accepted 9th March 2012
DOI: 10.1039/c2gc35309a

A one-pot, hydrothermal synthesis of nitrogen and sulfur dual doped carbon aerogels is presented, derived from our previously published hydrothermal carbonization approach. Two co-monomers, *S*-(2-thienyl)-L-cysteine (TC) and 2-thienyl carboxaldehyde (TCA), were used for sulfur incorporation, giving rise to distinct morphologies and varying doping levels of sulfur. Nitrogen-doping levels of 5 wt% and sulfur-doping levels of 1 wt% (using TCA) to 4 wt% (using TC) were obtained. A secondary pyrolysis step was used to further tune the carbon aerogel conductivity and heteroatom binding states. By comparing solely nitrogen-doped with nitrogen- and sulfur-doped carbon aerogels, it was observed that the presence of sulfur improves the overall electrocatalytic activity of the carbon material in both basic and acidic media. This study of the synergistic effect of combined sulfur- and nitrogen-doping in the catalysis of the "oxygen reduction reaction" (ORR) is expected to be significant to future research concerning the improvement of heterogeneous, metal-free, carbon-based catalysts.

Introduction

Carbon-based material technologies have made remarkable progress in recent years.[1–4] Their wide availability as well as diversity of physicochemical properties, such as chemical and thermal stability, electrical conductivity, and the ability to adopt a wide range of morphologies makes them highly attractive candidates for applications in sorption, chromatography, energy storage[1,3] and catalysis.[5–7] For most of these applications, high surface areas and porosity are desirable properties.[2,8] In this sense, carbon aerogels are interesting candidates, as they provide a very simple, template-free route towards coherent, low bulk density solids.[9] Organic aerogels have been previously prepared *via* the well-established resorcinol–formaldehyde (RF) route of Pekala[10] Recently, our group published a sustainable synthesis of nitrogen-doped carbon aerogels obtained by the hydrothermal carbonization[4] of glucose in the presence of a protein, ovalbumin.[11] In this context, incorporation of nitrogen has been used extensively to moderate carbon material properties for specific applications. Specifically in the context of electrocatalysis (*e.g.* fuel cells) where the dominance of platinum-based catalysts effectively hampers commercialisation, nitrogen-containing carbons based on Co-phthalocyanine were first proposed by Jasinski in 1964 as non-noble metal catalysts for the oxygen reduction reaction (ORR).[6] Since then, significant research efforts have focused on the development of non-noble metal,[12–17] but also metal-free, oxygen reduction catalysts.[18–24] Liu *et al.* pointed out the importance of the development of doped carbon materials without any metal components to help elucidate the correlation between structure, composition and electrochemical activity of nitrogen-doped carbon materials.[18] Regarding the heteroatom-doping of carbon structures, the effects of sulfur incorporation conversely has been less investigated, and similarly there are very few reports on carbon materials that are simultaneously doped with nitrogen and sulfur. Vulcan, one of the main commercial carbon supports, contains traces of thiophene-like sulfur but is normally desulfurized by the platinum catalyst during the processing of membrane-electrode assemblies for fuel cells.[8] Baker *et al.* functionalized RF aerogels with thiophenic sulfur moieties to maximize platinum uptake.[25] Very recently, Yang *et al.* reported on sulfur doped graphene (derived from annealing graphene-oxide and benzyl disulfide) as a highly efficient metal-free catalyst for the ORR in alkaline medium.[26] Choi *et al.* prepared nitrogen- and sulfur-doped carbons *via* the pyrolysis of cysteine in the presence of metal chlorides and showed their superior performance over purely nitrogen-doped carbons prepared from other amino acids.[23] However, their materials exhibited varying morphologies, making a direct comparison difficult,

[a]*Max Planck Institute of Colloids and Interfaces, Am Mühlenberg 1, 14467 Potsdam, Germany. E-mail: stephanie.wohlgemuth@mpikg.mpg.de; Fax: +49-331-56-9502; Tel: +49-331-567-9562*
[b]*Department of Inorganic Chemistry, Fritz Haber Institute of the Max Planck Society, Berlin, Germany*

†Electronic supplementary information (ESI) available: SEM, TEM, XPS and N_2 sorption data as well as details of physical and chemical sample characterization. See DOI: 10.1039/c2gc35309a

and due to the metal dependent synthesis the catalytic effect of trace metals in the final product cannot be fully excluded. We recently published a hydrothermal synthesis of sulfur- and nitrogen-doped carbon microspheres, though their application as ORR catalysts was not feasible due to a lack of surface area and developed porosity.[27] Herein a simple, metal-free route towards nitrogen- and sulfur-doped, high surface area carbon aerogels based on our glucose–ovalbumin system is presented.[11] Sulfur incorporation is achieved *via* the addition of *S*-(2-thienyl)-L-cysteine (TC) or 2-thiophene carboxaldehyde (TCA) to the hydrothermal carbonization recipe. The two different sulfur-containing aerogels are then tested for their ORR-related catalytic activity in both acidic and basic media, and their activities are compared to a solely nitrogen-doped aerogel made in an otherwise similar fashion, as well as to the common standards, Vulcan and platinum supported on Vulcan. In this way, we are able to show that the presence of sulfur, in addition to nitrogen, improves the overall electrocatalytic activity of the carbon aerogels in acidic and basic media, whereby the morphological aspects of the aerogels also play an important role. To the best of our knowledge, this is the first report on the *in situ* sulfur-doping of carbon aerogels *via* a green and sustainable biomass-based approach and hence the first time that nitrogen and sulfur dual-doped carbon aerogels were tested as fuel cells catalysts.

Experimental methods and sample characterization

Hydrothermal synthesis of aerogels

D-(+)-Glucose was purchased from Roth chemicals. *S*-(2-Thienyl)-L-cysteine (TC), 2-thienyl-carboxaldehyde (TCA), L-cysteine (CS), and lyophilized albumin powder (from chicken egg white) were purchased from Sigma Aldrich. All chemicals were used as received.

In a typical experiment, 1.5 g glucose and 0.3 g ovalbumin were dissolved in 13.5 g distilled water. For the sulfur doped aerogels, 1 mmol of the sulfur source (0.2 g for TC and 0.1 g for TCA) was added to the mixture. The solution was filled into a glass inlet which was then placed in a Teflon lined, stainless steel autoclave (45 ml volume, purchased from Parr Instruments). The autoclave was placed in a pre-heated furnace at 180 °C for 5.5 h after which it was allowed to cool down to room temperature. The resulting hydrothermal monoliths were washed with excess water and ethanol, followed by supercritical CO_2 drying to yield a low density carbonaceous aerogel. The samples were labeled CA, CA-TC and CA-TCA for the undoped, TC, and TCA containing aerogels, respectively.

For pyrolysis, the dried sample was placed in a ceramic crucible and covered with a ceramic lid. The crucible was placed in a nitrogen atmosphere furnace and flushed for 30 minutes before heating to 900 °C at a heating rate of 10 K min^{-1}. The final temperature was kept for 4 h, after which the furnace was allowed to cool to room temperature. The obtained black monoliths were ground to fine powders prior to further characterization. The suffix _900 was added to the corresponding sample labels.

Physical and chemical characterization

Extensive experimental characterization details are provided with the ESI.†

Results and discussion

The hydrothermal carbonization (HTC) of pure glucose at T = 180–200 °C, typically yields amorphous, non-porous carbon microspheres composed of a largely polyfuranic framework and abundant surface oxygen functional groups (*e.g.*, hydroxyl, carboxylic acid, lactones, *etc.*).[4,28–31] A simplified reaction mechanism involves the initial dehydration of glucose to hydroxymethylfurfural and other intermediates and their subsequent polymerization. More detailed explanations of the mechanism have been provided by the groups of Baccile and Titirici *et al*.[31,32] When nitrogen containing molecules are present, such as ovalbumin (which contains free amino side chains and whose peptide bonds may be hydrolyzed under hydrothermal conditions, giving rise to additional free amines), Maillard type reactions can take place.[33] In the glucose–ovalbumin system, ovalbumin (and associated Maillard products) act as surface stabilizing/structure directing agents for the formation of flexible heteroatom-doped carbon scaffolds. It is further assumed that part of the gelation process involves the crosslinking of forming hydrothermal particles by the ovalbumin-derived amino groups. Initial experiments using CS as the sulfur source resulted in micrometer sized spherical particles, which are very similar to those obtained when glucose is hydrothermally treated with cysteine without ovalbumin.[27] The amino and thiol groups in CS are thought to compete with the crosslinking process of ovalbumin and thereby prevent gel formation. Because the obtained product had neither defined structure nor high surface area, CS was not further used as a dopant molecule (ESI†, Fig. S1).

However, the addition of both *S*-(2-thienyl)-L-cysteine (TC) and 2-thienyl-carboxaldehyde (TCA) to the originally reported glucose–ovalbumin mixture successfully resulted in monolith formation. The as-synthesized aerogels were dried in supercritical CO_2 in order to preserve as high as possible the metastable hydrogel state and avoid capillary force-induced collapse of the 3-dimensionally ordered nano-architectures. Comparatively, freeze drying is a more convenient option, but usually results in lower surface areas. Transmission electron microscopy (TEM) images show that the morphologies obtained depend on which additive/co-monomer is used (Fig. 1). Addition of TC gives rise to larger spherical particles (*ca.* D = 200 nm) which are linked to a smaller particle matrix (Fig. 1b). Addition of TCA results in a homogeneous interconnected particle matrix only (Fig. 1c) and the morphology is similar to that seen for the original nitrogen-doped CA (Fig. 1a). The difference in morphology of CA-TC is attributed to heterogeneous nucleation and structure formation, in accordance with the LaMer model. A heterogeneous morphology with larger discrete particles and an interconnected particle matrix is the result. With TCA, the incorporation of sulfur presumably takes place exclusively *via* electrophilic aromatic substitution or cycloaddition, and crosslinking can proceed unhindered. Nitrogen sorption data are in good agreement with the TEM image analysis. The sulfur and nitrogen doped carbon aerogels after HTC at 180 °C exhibit Type IV/H3 reversible

sorption isotherms with limited hysteresis loop profiles (Fig. 2a). The lack of an adsorption plateau at high relative pressures as well as the broad pore size distribution for all samples are indicative of slit shaped pores in an open pore system (Fig. 2b).[11] These results are similar to those described for CA by White *et al.*, although in the case of CA-TCA the BET surface area is lower than in CA and in CA-TC (Table 1).[11] The large increase in the nitrogen volume adsorbed p/p_0 approaches unity, particularly for CA-TC it is attributed to the condensation of adsorbate in large mesopores or (very small) macropores within the continuous coral-like material architecture. CA-TC has the largest mesopore volume among the three samples (0.46 $cm^3\ g^{-1}$, *cf.* ~0.30 $cm^3\ g^{-1}$ for CA and CA-TCA), a result of the observed change in material morphology with precursor chemistry. This is also reflected in the pore size distributions of the samples (Fig. 2). Whilst pore size distributions demonstrate that volume levels off after a pore width of *ca.* 20 nm for CA and CA-TCA, that of CA-TC shows a secondary increase towards still larger pores. The simultaneous incorporation of nitrogen and sulfur into the HTC-derived carbons was confirmed by elemental analysis and X-ray photoelectron spectroscopy (XPS) (Table 1). The carbon content is slightly increased for the nitrogen and sulfur containing carbon aerogels. The additional nitrogen in the co-monomer TC does not influence the final nitrogen content of CA-TC (5.87 wt%) compared to CA-TCA (5.47 wt%) significantly, indicating that the predominant source

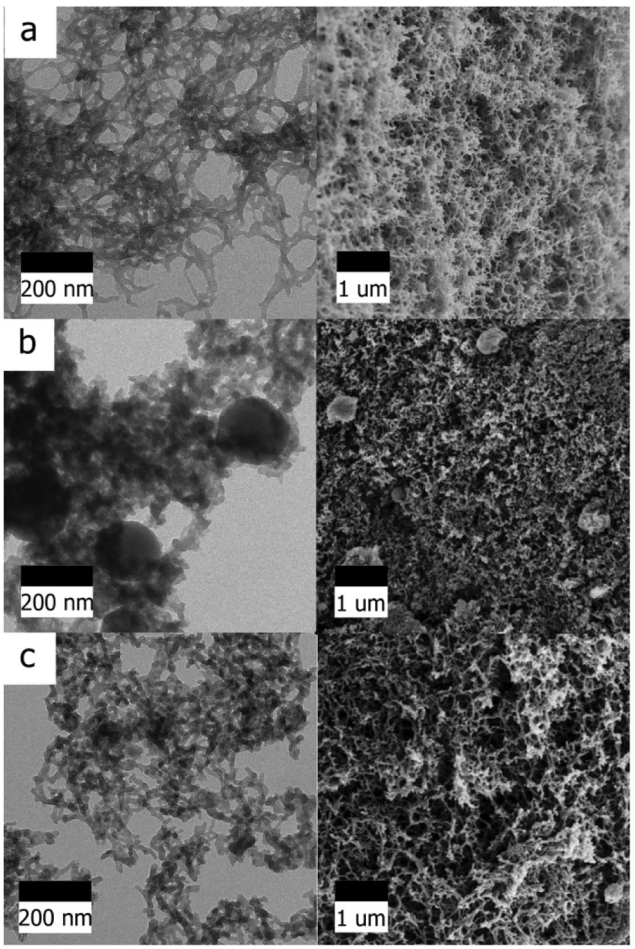

Fig. 1 TEM (left) and SEM (right) images of (a) CA; (b) CA-TC; (c) CA-TCA.

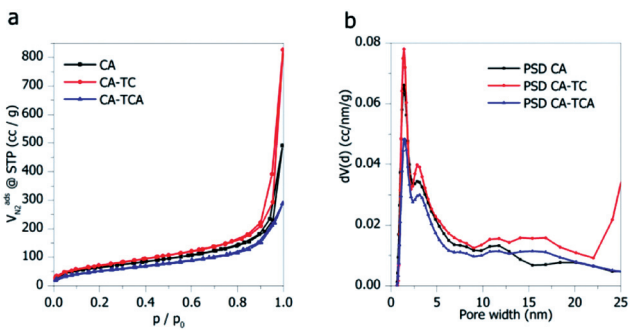

Fig. 2 (a) Nitrogen sorption isotherms and (b) pore size distributions (QSDFT model) obtained for aerogels after HTC at 180 °C.

Table 1 Elemental composition of the bulk and surface of the aerogels after HTC at 180 °C and after pyrolysis at 900 °C, determined by elemental analysis and XPS, respectively. [NB: N_2 sorption-derived textural and electrical conductivity properties of the presented materials are shown on the right]

	Elemental composition by EA (wt%) and *XPS (at %)*					Textural properties				
Sample	C	H	N	S	S/N	S_{BET} ($m^2\ g^{-1}$)	V_{total} ($cm^3\ g^{-1}$)	V_{meso} ($cm^3\ g^{-1}$)	V_{micro} ($cm^3\ g^{-1}$)	Σ(S m^{-1})
CA	61.75	5.53	5.89	1.12	0.19	238.9	0.34	0.28	0.06	—
	72.3	—	*6.8*	*0.5*	*0.1*					
CA-TC	59.79	5.39	5.87	3.82	0.65	262.8	0.52	0.46	0.06	—
	73.4	—	*5.4*	*1.6*	*0.3*					
CA-TCA	58.40	5.25	5.47	1.71	0.31	188.8	0.33	0.29	0.04	—
	74.2	—	*4.6*	*1.1*	*0.2*					
CA_900	88.48	0.79	5.33	0.11	0.02	266.7	0.47	0.40	0.07	468.2
	93.2	—	*3.6*	—	—					
CA-TC_900	87.15	0.99	4.28	1.04	0.24	321.3	0.48	0.38	0.09	660.2
	93.6	—	*3.5*	*0.7*	*0.2*					
CA-TCA_900	86.50	0.84	4.96	0.74	0.15	224.5	0.27	0.20	0.07	503.6
	93.1	—	*3.3*	*0.5*	*0.2*					

σ = specific conductivity as determined by impedance spectroscopy.

of the nitrogen is the protein. Notably CA-TC contains more than twice the amount of sulfur than CA-TCA (3.82 wt% for CA-TC compared to 1.71 wt% for CA-TCA). The S/N ratios are similar for (surface) XPS but vary greatly when compared to the (bulk) elemental analysis data. For the presented HTC aerogels prepared at 180 °C, the elemental analysis-derived S/N ratios typically exceed the XPS-derived ones. Such deviations are very typical and are related to the fact that elemental analysis detects all sulfur atoms, while XPS is a surface sensitive technique and therefore reflects surface enrichment of functional groups. The bulk/surface ratio of sulfur, given by $sulfur_{EA}/sulfur_{XPS}$ for CA-TC (2.39) is much higher than for CA-TCA (1.55). On the other hand, the bulk/surface ratios of nitrogen, given by $nitrogen_{EA}/nitrogen_{XPS}$, are similar (1.09 for CA-TC and 1.19 for CA-TCA) and much closer to unity, indicating the absence of surface depletion or enrichment. Hence, CA-TC contains the majority of sulfur atoms in the bulk while the bulk and surface sulfur species in CA-TCA are more balanced. It is very possible that some of the sulfur species in CA-TC are trapped within the species of larger particles, since this morphological feature is coupled to the presence of this sulfur source. In contrast, CA-TCA exhibits a uniform morphology and all the sulfur atoms are therefore better dispersed throughout the gel matrix. A larger proportion of surface sulfur implies catalytically accessible sites, while bulk sulfur can contribute only indirectly by the altered electronic properties of carbon. Interestingly, also CA contains minor amounts of sulfur, arising from the cysteine moieties of ovalbumin.[34] Cysteine, however, cannot undergo cyclo-addition with HTC intermediates and is therefore only weakly incorporated within the carbon framework. It was previously observed that the predominant species here are aliphatic thiols or oxidized sulfur groups.[27]

Overall, all CA, CA-TC and CA-TCA exhibit promising structures and compositions for catalytic applications, such as high surface areas, large diameters, continuous 3-dimensionally arranged porous morphologies (and hence good mass transfer properties) leading to accessible dopant sites. However, the amorphous nature of hydrothermal carbon directly after HTC at 180 °C has the drawback of a rather low electrical conductivity. In order to convert the "organic aerogels" into "carbon aerogels" which are suitable for electrocatalytic applications, a pyrolysis step at 900 °C was added to the synthesis process.

Following this temperature treatment (under an inert atmosphere), X-ray diffraction (XRD) shows two main peaks for the pyrolized carbon aerogels (Fig. 3d). The peaks at around 22°–23° and at 43.5° are the equivalents of the hexagonal graphite 002 (2Θ = 26°) and 100 (2Θ = 43°) reflections, respectively.[35] However, the large shift towards smaller angles for the 002 reflection implies a significant increase in the interlayer spacing. The shift is more pronounced for the sulfur containing samples (22.5° for CA-TC_900 and CA-TCA_900 compared to 23.1° for CA_900), and can be directly related to the much larger size of the sulfur atom, as compared to carbon or nitrogen.[36–38] The

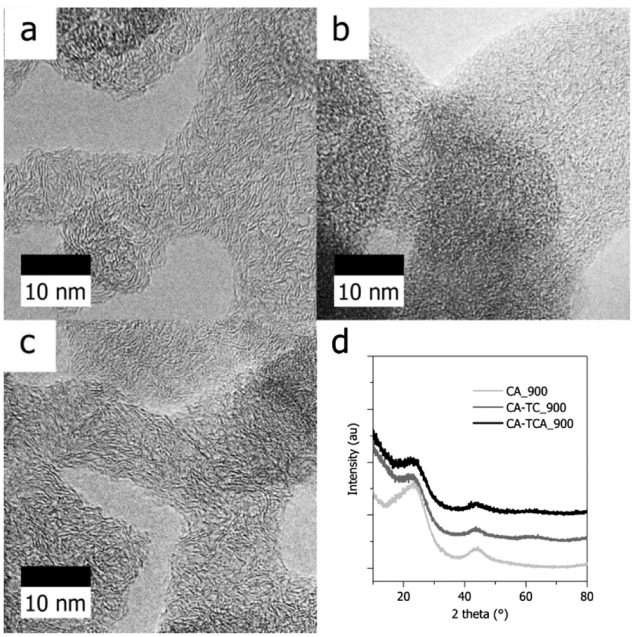

Fig. 3 HRTEM images of (a) CA_900; (b) CA-TC_900 and (c) CA-TCA_900. (d) Powder XRD patterns for the pyrolized carbon aerogels.

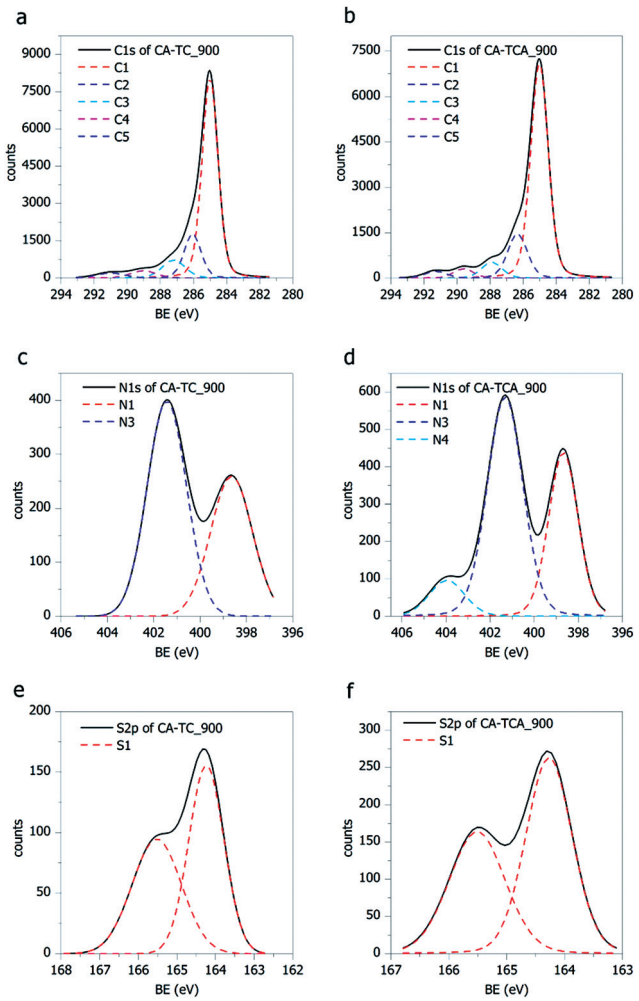

Fig. 4 Deconvoluted C1(s), N1(s) and S2(p) photoelectron envelopes of CA-TC_900 (a, c and e, respectively), and CA-TCA_900 (b, d and f, respectively).

result of this heat treatment leads to the specific conductivity values for the pyrolized aerogels increasing in the order CA_900 < CA-TCA_900 < CA-TC_900, *i.e.* sulfur doped carbons are better electronic conductors (Table 1). TEM images show that the promising continuous 3-dimensional architecture is nicely retained after pyrolysis, whereby a slight contraction of the interconnected particle matrix occurs due to the further condensation and graphitization of the carbon framework (ESI†, Fig. S2). High resolution TEM (HRTEM) images show disordered, highly bent graphitic layers, typical of doped carbon materials (Fig. 3a–c).[11,37,38] These defects may be beneficial for catalytic activity due to facilitated chemisorption of reactants at the sterically less hindered active sites.[39]

The nitrogen sorption isotherms of the pyrolized aerogels exhibit the same type IV/H3 profile as the as-synthesized aerogels (ESI† Fig. S3a), but with a slightly more pronounced hysteresis feature, indicating more (mesoporous) cavities in the more rigid carbon structure; presumably the result of overall dimensional shrinkage and the number of mesopores in the lower "meso" diameter region. The aerogel surface areas increase upon pyrolysis, due to the loss of micropore-bound decomposition products (Table 1).[11] Again, the TCA containing sample presented the lowest surface area and pore volumes (Table 1). There is a possibility of pore shrinkage after carbonization at 900 °C which explains the only moderate increase in aerogel surface areas.[27]

Concerning the elemental composition of the pyrolized samples, the S/N ratios now agree well between XPS and elemental analysis (Table 1). This indicates that heating has homogenized the sulfur distribution between bulk and surface, presumably *via* the loss of pendant, weakly bound sulfur species. CA_900 has lost virtually all sulfur species, which is consistent with the statement earlier that cysteine as sulfur source does not result in stable, structurally bound sulfur moieties. The aliphatic sulfur groups are easily lost upon heat treatment.

Fig. 4 shows the deconvoluted C1(s,) N1(s) and S2(p) photoelectron envelopes of CA-TC_900 (Fig. 4a, b and c, respectively), and CA-TCA_900 (Fig. 4d, e and f, respectively). The corresponding data for CA-TC and CA-TCA can be found in ESI†, Fig. S4. The peak assignments are summarized in Table 2, whereby the fraction of different species (in %) is shown in grey. Following the mechanistic discussions earlier in this article, it is no surprise that the majority of sulfur species are structurally bound (*i.e.*, thiophenic sulfur, assigned as S1) already in the as-synthesized aerogels. In this regard, the "sulfur" precursor sources were chosen due to their ability to interact with the albumin/glucose HTC intermediates *via* electrophilic aromatic substitution or cycloaddition. This leads to sulfur bound structurally within the carbonaceous framework, as opposed to pending sulfur functionalities (*e.g.*, thiol).[27] After pyrolysis at 900 °C, practically all surface sulfur atoms are bound in a thiophenic fashion. For nitrogen, a transformation of pyrrolic nitrogen (N2) in the as-synthesized aerogels towards more stable pyridinic (N1) and quaternary (or graphitic, N3) nitrogen is observed, similar to the results published on other N-doped carbons.[11] In the case of CA-TCA_900, 9.2% of surface nitrogen species are present as pyridinic-*N*-oxide (N4). Oxidation may occur as a result of oxygen species, generated during heat treatment, reacting with surface heteroatoms. The major fraction of carbon species is sp^2 hybridized (C1), and the appearance of a π–π* shake up satellite (C5) after pyrolysis clearly shows that further carbonization and aromatization take place during the heat treatment, rendering the carbonaceous materials electrically conducting.

Electrochemical characterisation

CA_900, CA-TC_900 and CA-TCA_900 were tested for their electrocatalytic activity in the oxygen reduction reaction (ORR) of fuel cells in both alkaline and acidic media. Three main points had to be investigated:

The *general catalytic activity of CA_900*. Material synthesis and characterization of nitrogen doped carbon aerogels has been presented before, but no applications for the materials were presented. The catalytic activity of CA_900 is compared to a commercially available platinum catalyst (20 wt% Pt@C) and also to pure Vulcan carbon.

The *effect of sulfur-doping in addition to nitrogen-doping*, *i.e.*, the catalytic activity of CA-TC_900 and CA-TCA_900 is compared to solely nitrogen doped CA_900.

The *effect of the morphological difference* between CA-TC_900 and CA-TCA_900.

Cyclic voltammetry at a scan rate of 100 mV s^{-1} and rotating disk electrode (RDE) voltammetry at a scan rate of 10 mV s^{-1}

Table 2 Peak assignments for the C1(s), N1(s) and S2(p)3/2 photoelectron envelopes for CA-TC and CA-TCA samples after HTC at 180 °C and after subsequent pyrolysis at 900 °C

	Binding energy (eV)/fraction of species (%)				
Peak	CA-TC	CA-TC_900	CA-TCA	CA-TCA_900	Assignment
C1s	285.00/52.1	285.00/67.8	285.00/53.8	285.00/86.0	C1 sp^2 C–C or C–H[23,40,41]
	286.30/32.4	286.10/16.0	286.40/28.5	286.20/18.2	C2 C–O/C–N/C–S[23]
	287.89/10.0	287.20/9.0	288.10/14.3	287.70/7.0	C3 C=O/C=N[23,42]
	289.10/5.5	289.00/4.1	289.70/3.1	289.56/4.4	C4 O=C–O[43]
	—	291.00/3.2	—	291.35/2.3	C5 π–π* shake up satellite[41,44]
N1s	—	398.60/40.9	—	398.68/34.6	N1 pyridinic[41,45]
	400.20/100.0	—	400.20/100.0	—	N2 pyrrolic[45]
	—	401.40/59.1	—	401.30/56.2	N3 quaternary[23,45]
	—	—	—	403.96/9.2	N4 pyridinic *N*-oxide[23]
$S2p_{3/2}$	164.10/84.5	164.20/100.0	164.30/83.2	164.27/100.0	S1 thiophenic (aromatic) C–S–C[40,46]
	166.80/15.5	—	168.10/16.8	—	S2 oxidized sulfur[40,46]

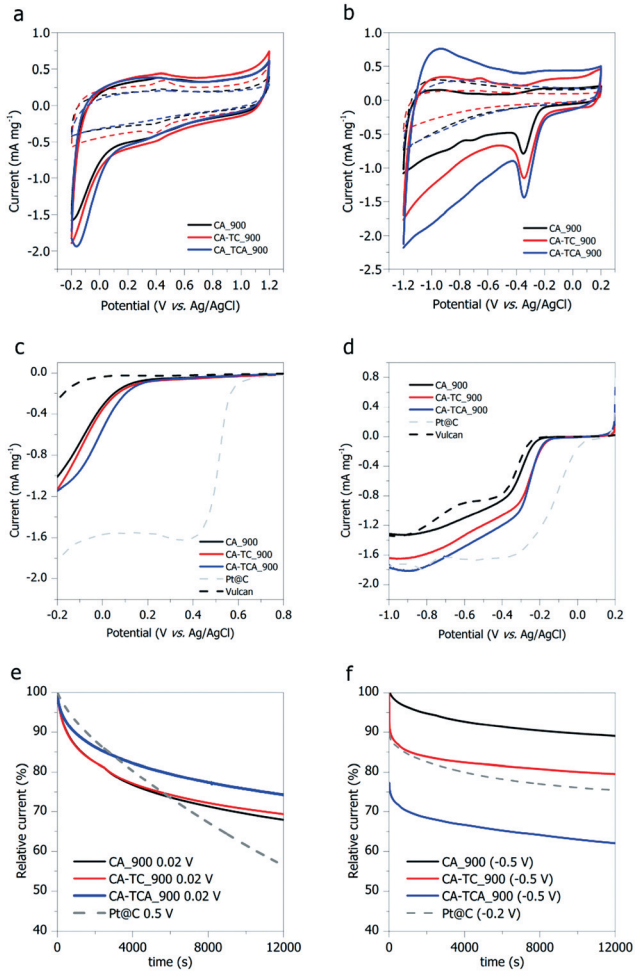

Fig. 5 Cyclic voltammograms of doped carbon aerogels compared to Pt@C and Vulcan in (a) 0.1 M $HClO_4$ and (b) 0.1 M KOH. RDE polarization curves at C a 1600 rpm of doped carbon aerogels compared to 20 wt% Pt@C and Vulcan in (c) 0.1 M $HClO_4$ and (d) 0.1 M KOH. Chronoamperic responses over 12 000 s at a constant rotation speed of 1600 rpm in O_2-saturated solution of doped carbon aerogels compared to Pt@C in (e) 0.1 M $HClO_4$ and (f) 0.1 M KOH.

were conducted in 0.1 M KOH and 0.1 M $HClO_4$ (Fig. 5a and b). In both cases, featureless voltammetric curves are observed for all doped carbon aerogels in the N_2-saturated solution. The area of the voltammograms arises from capacitive currents of the electrodes. In contrast, a well-defined cathodic peak appears in the O_2-saturated 0.1 M KOH solution (Fig. 5b), clearly demonstrating the electrocatalytic activity of the doped carbon aerogels towards oxygen reduction. The areas of the voltammograms are larger in O_2-saturated solution due to Faradaic currents (*i.e.*, current generated by charge transfer between reacting species). In 0.1 M $HClO_4$, Faradaic currents are similarly observed for the doped aerogels O_2-saturated solution (Fig. 5a). Because the aerogels are less active in acidic than in alkaline media, the pronounced cathodic peaks found in 0.1 M KOH are not visible in 0.1 M $HClO_4$ at the same scan rate of 10 mV s^{-1}. The small redox peaks observed for CA_900 and CA-TC_900 in N_2-saturated solution may be a result of heteroatom protonation on the carbon surface. The polarization curves obtained from RDE

Table 3 Summary of values derived from linear sweep voltammetry and chronoamperometry measurements using a rotating disk electrode in O_2-saturated 0.1 M $HClO_4$ and 0.1 M KOH

	Electrochemical characterization in 0.1 M $HClO_4$–0.1 M KOH		
Sample	Onset potential (mV *vs.* Ag/AgCl)	Max. current density (mA mg^{-1})	Rel. current after 12 k s CA (%)
CA_900	>200/−185	1.01[a]/1.32[b]	68/89
CA-TC_900	>200/−130	1.14[a]/1.65[b]	70/80
CA-TCA_900	>200/−130	1.14[a]/1.82[b]	74/62
Pt@C	670/80	1.78[a]/1.73[b]	56/75
Vulcan	33/−220	0.26[a]/1.32[b]	—

[a] At −0.2 V *vs.* Ag/AgCl. [b] At −0.9 V *vs.* Ag/AgCl.

(1600 rpm) voltammetry in O_2-saturated 0.1 M $HClO_4$ and 0.1 M KOH are shown in Fig. 5c and d, respectively. A summary of values derived from the plots is given in Table 3. In 0.1 M $HClO_4$, both onset potential and maximum current density are significantly improved for all doped carbon aerogels relative to pure Vulcan. Compared to Pt@C however, the aerogels are still not competitive. In 0.1 M KOH, the performance of the doped aerogels is far more comparable with that of Pt@C. Compared to Vulcan, CA_900 shows an improved onset potential of −185 mV as well as slightly improved current densities within the scanned potential range. The onset potential of the sulfur and nitrogen containing aerogels is more positive (both at around −130 mV) and the maximum current density is considerably higher than for Vulcan.

The chronoamperic responses (12 000 s at a constant rotation speed of 1600 rpm) of all aerogels and Pt@C in O_2-saturated 0.1 M $HClO_4$ and 0.1 M KOH are shown in Fig. 5e and f, respectively. All aerogels exhibit better stability than Pt@C in 0.1 M $HClO_4$. The stability decreases in the order CA-TCA_900 > CA-TC_900 > CA_900. Interestingly, this order is reversed in 0.1 M KOH, *i.e.*, the most active aerogel now has the lower stability, with the relative current decreasing to about 62% after 12 000 s. CA_900 on the other hand shows remarkable stability, retaining roughly 89% of the initial current. CA-TC_900 retains around 80%, which is, however, still slightly higher than Pt@C (75%). Importantly, the presented simultaneously nitrogen- and sulfur-doped aerogels show an enhanced overall performance over the solely nitrogen-doped aerogel. It is a little surprising that CA-TCA_900, which has a lower surface area, sulfur content, and is also less conductive than CA-TC_900, shows the overall best performance. Further experiments are underway to identify the reasons for this behavior, but might be related to the presence of specific surface sites. The distribution of sulfur and nitrogen in CA-TCA_900 is homogeneous, as was confirmed by EDX mapping shown in Fig. 6. Assuming that the sulfur sites are more prone to oxidation or decomposition reactions, this would also explain the order of durability in 0.1 M KOH (most active catalyst is the least stable). An explanation for the reverse trend in acidic conditions is, however, still required. One possibility would be that the sulfur and/or nitrogen groups are protonated in acidic media. This would render them chemically more stable compared to the more reactive form in alkaline media.

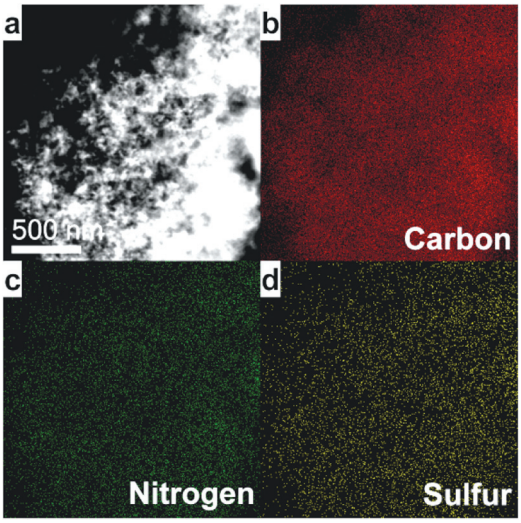

Fig. 6 EDX mapping of CA-TCA_900. (a) Dark field STEM image of the sample area on which mapping was carried out. (b) Carbon map; (c) nitrogen map, (d) sulfur map; the heteroatoms are homogeneously dispersed throughout the investigated sample area.

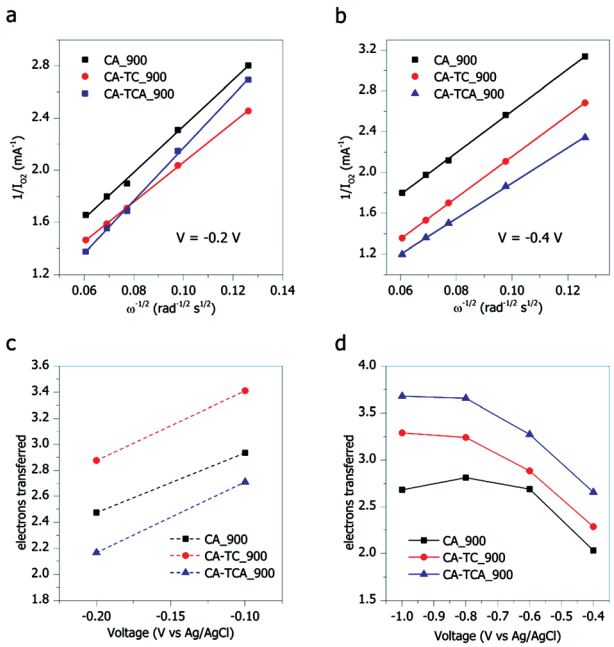

Fig. 7 Koutecky–Levich plots in (a) 0.1 M $HClO_4$ at −0.2 V; (b) 0.1 M KOH at −0.4 V. Transferred electrons as determined by Koutecky–Levich plots at various voltages in (c) 0.1 M $HClO_4$, and (d) 0.1 M KOH.

This interpretation, however, seems inconsistent with the order of catalytic activity, which is the same as in 0.1 M KOH.

Another important factor concerning ORR catalysts is whether the mechanism goes *via* a 2 electron (forming H_2O_2 as an intermediate) or a 4 electron process, and how selectively this occurs. Platinum usually catalyzes a 4 electron process, which is desired for efficient operation of a fuel cell.[47] Fig. 7 shows the Koutecky–Levich plots of the doped carbon aerogels in 0.1 M $HClO_4$ (at −0.2 V) and 0.1 M KOH (at −0.4 V), as well as number of electrons transferred during the catalytic reaction at various voltages. The Koutecky–Levich plots show good linearity, though the mechanism for the carbon aerogels is not very selective for either the 2 or 4 electron process, but seems to comprise a mixture of the two (Fig. 7a and b). In 0.1 M $HClO_4$, the selectivity tends towards a 2 electron process with decreasing voltages (Fig. 7c). In 0.1 M KOH, the opposite is observed, *i.e.*, the electron transfer number tends towards 4 with decreasing voltages (Fig. 7d). This means that sulfur-doping not only improves catalytic performance, but also the selectivity towards a 4 electron process in 0.1 M KOH, and towards a 2 electron process in 0.1 M $HClO_4$. Note that selective 4 electron mechanisms are important for the ORR in fuel cells, because H_2O_2 can poison the cell. Selective 2 electron processes, however, are also of great interest outside the context of ORR, namely for the electrochemical synthesis of H_2O_2.[48] Overall, the above findings provide indirect evidence that a small amount of sulfur-doping (0.74 wt% in the case of CA-TCA_900) is sufficient to generate profound effects on the electrocatalytic activity of carbon-based electrodes. The current knowledge in the scientific literature regarding sulfur and ORR is limited, and sulfur is usually thought to improve Pt particle adsorption onto carbon supports and thereby the lifetime of the electrode.[25] But what is the role of sulfur in metal-free catalysts, and how does sulfur compare to nitrogen as a dopant? In nitrogen-doped carbons, factors such as enhanced π-bonding, electrical conductivity and Lewis basicity may facilitate reductive O_2 adsorption at the carbon surface.[49] Structural defects in the carbon crystal lattice, which are caused by the introduction of dopants, also result in more edge-active sites.[21] It has, however, been shown that undoped carbon materials with more edge sites did not have an improved catalytic performance,[50] indicating that edge-bound heteroatoms, (*e.g.*, pyridinic nitrogen), are catalytically important. It is generally accepted that the binding state is relevant with respect to the catalytic activity of nitrogen, though there are different opinions as to which exact binding states are responsible for the good activity and 2 or 4 electron process selectivity. Pyridinic edge sites have been proposed as a likely candidate because edge planes facilitate oxygen chemisorption.[39] On the other hand, some reports also suggest that pyridinic nitrogen may not be an effective promoter of the 4 electron ORR process. Luo *et al.* synthesized purely pyridinic nitrogen doped carbons and found them to be selective for a 2 electron reduction pathway.[51] Lui *et al.* recently proposed that graphitic nitrogen accounts for good catalytic activity. They also showed that the nitrogen content does not directly correlate with the catalyst performance – materials (nitrogen-doped mesoporous graphitic arrays) with higher nitrogen content showed lower selectivity and activity.[18] A report by Strelko *et al.* suggested that there is a critical concentration of heteroatoms in a carbon matrix which will exhibit maximum catalytic activity and that this can be explained by the collective electronic properties and a minimal bandgap. They identified pyrrolic nitrogen as the binding state that gives rise to the smallest bandgap, and thus the best electron transfer capabilities.[52] DFT calculations suggest that nitrogen is not itself the catalytically active site, but that the high electronegativity of nitrogen polarizes the C–N bond, and the adjacent carbon atom therefore has a reduced energy barrier towards ORR.[21,53] In our

opinion, the many attempts to identify a mechanism for the catalytic activity of nitrogen doped carbons have yielded many different and sometimes contradicting interpretations, and a definite answer remains missing. It is possible that the catalytic mechanism of nitrogen-doping is dependent on the electronic and morphological features of the material, so that a single definite catalytic pathway does not exist.

Coming back to the present case of sulfur-doping, for which much less information is available, an unambiguous mechanistic proposition is clearly difficult. Some properties of sulfur can be compared to nitrogen:

Electronegativity. Sulfur and carbon have electronegativities of 2.58 and 2.55, respectively (on the Pauling scale). Nitrogen on the other hand has an electronegativity of 3.04. This means that the C–S bond is not as polarized as the C–N bond, so a catalytic pathway based on a δ + adjacent carbon atom is unlikely to occur for sulfur.

Size. Sulfur is a large atom with an atomic radius of 100 pm compared to nitrogen (65 pm) and carbon (70 pm).[36] The disruption of the carbon connection pattern is therefore more pronounced than for nitrogen, as also seen by the larger interlayer spacing from XRD measurements. It is therefore likely that sulfur-doping will induce more strain and defect sites in the carbon material, which may facilitate charge localization and the coupled chemisorption of oxygen.

Polarizability. Sulfur has large, polarizable d-orbitals (sulfur groups are usually soft nucleophiles). The lone pairs of sulfur can therefore easily interact with molecules in the surrounding electrolyte. This effect is expected to be much more pronounced than that for nitrogen.

If we favour the "indirect" catalytic mechanism for nitrogen doped carbons, *i.e.*, that the active site is in fact the δ + carbon atom adjacent to nitrogen, it is immediately clear that the mechanism for sulfur-doping cannot be the same as for nitrogen. Sulfur is, however, known to take part in proton transfer reactions. DFT calculations carried out by Chamorro *et al.* suggested that proton transfer in thiooxalic acid derivatives is facilitated by the high polarisability of the sulfur atom, which mediates ion-pair like transition states during the transfer process.[54] Scheiner *et al.* carried out *ab initio* calculations and showed that the greater polarizability of SH_2 as compared to OH_2 leads to greater charge transfer between $(H_2S–H–SH_2)^+$ units than between $(H_2O–H–OH_2)^+$ units and to a larger extent of spatial regions of density charge.[55] In their publication on sulfur-doped graphene as ORR catalysts, Yang *et al.* propose that the increased spin density of sulfur compared to nitrogen or other dopants may be responsible for the increased catalytic activity.[26] This would mean that sulfur is favourable to interact with the triplet state of oxygen, as preservation of spin is a serious catalytic problem.

For our sulfur and nitrogen dual doped carbon aerogels, we tentatively propose a synergistic or consecutive mechanism between sulfur and nitrogen, whereby nitrogen activates the oxygen molecule (either directly or indirectly *via* the adjacent carbon atom), while sulfur facilitates the proton transfer during the reduction process.

Conclusion

In conclusion, we have presented a simple, one-pot synthesis for the preparation of dual sulfur and nitrogen-doped carbon aerogels based on sustainable precursors (*i.e.* glucose and ovalbumin). Our approach represents the first *in situ* synthesis towards sulfur and nitrogen dual doped aerogels. The positive effect of sulfur added to nitrogen-doping on the electrocatalytic performance in the oxygen reduction reaction in both acidic and basic media was demonstrated, whereby the carbon aerogels showed significantly enhanced activity in basic medium, as is typical for carbon materials. In acidic conditions all doped aerogels showed very good stability compared to a platinum based catalyst, as well as an activity which is still much better than ordinary carbon supports, but not competitive to the noble metal systems.

Koutecky–Levich plots showed that both 2 and 4 electron processes take place for all aerogels tested. Finally, we tentatively propose a synergistic mechanism between nitrogen and sulfur dopants, whereby nitrogen directly or indirectly (*via* the adjacent carbon atom) aids O_2 dissociation and sulfur facilitates proton transfer. While we appreciate that the herein presented materials currently do not show competitive catalytic activity with doped carbons, we emphasize that our findings strongly suggest that hydrothermal carbons are at least high potential candidates for future energy related applications. The sustainable and simple nature of the technique provides economic and environmental feasibility, a property which graphene and CNT based materials have yet to achieve. Also, given the small number of reports found in literature concerning dual doped carbon materials, the presented results encourage future research in this direction.

Acknowledgements

Philipp Jäker is acknowledged for relevant work carried out during his summer internship. Tim Fellinger, Nina Fechler and Xinchen Wang are acknowledged for scientific discussion. Sylvia Pirok, Heike Runge and Rona Pitschke are acknowledged for elemental analysis and SEM measurements. XPS analysis was carried out by Carmen Serra at the University of Vigo, Spain.

Notes and references

1 Y. Zhai, Y. Dou, D. Zhao, P. F. Fulvio, R. T. Mayes and S. Dai, *Adv. Mater.*, 2011, **23**, 4828–4850.
2 C. D. Liang, Z. J. Li and S. Dai, *Angew. Chem., Int. Ed.*, 2008, **47**, 3696–3717.
3 D. S. Su and R. Schlögl, *ChemSusChem*, 2010, **3**, 136–168.
4 M. M. Titirici and M. Antonietti, *Chem. Soc. Rev.*, 2010, **39**, 103–116.
5 P. Serp, M. Corrias and P. Kalck, *Appl. Catal., A–Gen.*, 2003, **253**, 337–358.
6 R. Jasinski, *Nature*, 1964, **201**, 1212–1213.
7 E. Guilminot, F. Fischer, M. Chatenet, A. Rigacci, S. Berthon-Fabry, P. Achard and E. Chainet, *J. Power Sources*, 2007, **166**, 104–111.
8 D. R. Rolison, *Science*, 2003, **299**, 1698–1701.
9 A. C. Pierre and G. M. Pajonk, *Chem. Rev.*, 2002, **102**, 4243–4266.
10 R. W. Pekala, *J. Mater. Sci.*, 1989, **24**, 3221–3227.
11 R. J. White, N. Yoshizawa, M. Antonietti and M.-M. Titirici, *Green Chem.*, 2011, **13**, 2428–2434.
12 H. R. Byon, J. Suntivich and Y. Shao-Horn, *Chem. Mater.*, 2011, **23**, 3421–3428.

13 H. Wang, Y. Liang, Y. Li and H. Dai, *Angew. Chem., Int. Ed.*, 2011, **50**, 10969–10972.
14 M. Lefevre, E. Proietti, F. Jaouen and J. P. Dodelet, *Science*, 2009, **324**, 71–74.
15 E. Proietti, F. Jaouen, M. Lefèvre, N. Larouche, J. Tian, J. Herranz and J.-P. Dodelet, *Nat. Commun.*, 2011, **2**, 416.
16 R. Bashyam and P. Zelenay, *Nature*, 2006, **443**, 63–66.
17 A. Morozan, B. Jousselme and S. Palacin, *Energy Environ. Sci.*, 2011, **4**, 1238–1254.
18 R. L. Liu, D. Q. Wu, X. L. Feng and K. Mullen, *Angew. Chem., Int. Ed.*, 2010, **49**, 2565–2569.
19 Y. F. Tang, B. L. Allen, D. R. Kauffman and A. Star, *J. Am. Chem. Soc.*, 2009, **131**, 13200–13201.
20 S. Yang, X. Feng, X. Wang and K. Müllen, *Angew. Chem., Int. Ed.*, 2011, **50**, 5339–5343.
21 H. Jin, H. Zhang, H. Zhong and J. Zhang, *Energy Environ. Sci.*, 2011, **4**, 3389–3394.
22 K. P. Gong, F. Du, Z. H. Xia, M. Durstock and L. M. Dai, *Science*, 2009, **323**, 760–764.
23 C. H. Choi, S. H. Park and S. I. Woo, *Green Chem.*, 2011, **13**, 406–412.
24 G. Liu, X. Li, J.-W. Lee and B. N. Popov, *Catal. Sci. Technol.*, 2011, **1**, 207–217.
25 W. S. Baker, J. W. Long, R. M. Stroud and D. R. Rolison, *J. Non-Cryst. Solids*, 2004, **350**, 80–87.
26 Z. Yang, Z. Yao, G. Li, G. Fang, H. Nie, Z. Liu, X. Zhou, X. A. Chen and S. Huang, *ACS Nano*, 2011, **6**, 205–211.
27 S.-A. Wohlgemuth, F. Vilela, M.-M. Titirici and M. Antonietti, *Green Chem.*, 2012, **14**, 741–749.
28 B. Hu, K. Wang, L. H. Wu, S. H. Yu, M. Antonietti and M. M. Titirici, *Adv. Mater.*, 2010, **22**, 813–828.
29 B. Hu, S. H. Yu, K. Wang, L. Liu and X. W. Xu, *Dalton Trans.*, 2008, 5414–5423.
30 M. M. Titirici, A. Thomas and M. Antonietti, *New J. Chem.*, 2007, **31**, 787–789.
31 M. M. Titirici, M. Antonietti and N. Baccile, *Green Chem.*, 2008, **10**, 1204–1212.
32 N. Baccile, G. Laurent, F. Babonneau, F. Fayon, M.-M. Titirici and M. Antonietti, *J. Phys. Chem. C*, 2009, **113**, 9644–9654.
33 S. K. Grandhee and V. M. Monnier, *J. Biol. Chem.*, 1991, **266**, 11649–11653.
34 T. X. Cui, R. Lv, Z. H. Huang, F. Y. Kang, K. L. Wang and D. H. Wu, *Nanoscale Res. Lett.*, 2011, **6**, 257–262.
35 Z. Q. Li, C. J. Lu, Z. P. Xia, Y. Zhou and Z. Luo, *Carbon*, 2007, **45**, 1686–1695.
36 J. C. Slater, *J. Chem. Phys.*, 1964, **41**, 3199–3205.
37 S. Glenis, A. J. Nelson and M. M. Labes, *J. Appl. Phys.*, 1999, **86**, 4464–4466.
38 Y. P. Wu, S. Fang, Y. Jiang and R. Holze, *J. Power Sources*, 2002, **108**, 245–249.
39 P. H. Matter, L. Zhang and U. S. Ozkan, *J. Catal.*, 2006, **239**, 83–96.
40 J. P. Paraknowitsch, A. Thomas and J. Schmidt, *Chem. Commun.*, 2011, **47**, 8283–8285.
41 Z. Li, N. Baccile, S. Gross, Z. Yuanjian, W. Wei, S. Yuhan, M. Antonietti and M. M. Titirici, *Carbon*, 2010, **48**, 3778–3787.
42 N. Baccile, M. Antonietti and M.-M. Titirici, *ChemSusChem*, 2010, **3**, 246–253.
43 M. Sevilla and A. B. Fuertes, *Chem.–Eur. J.*, 2009, **15**, 4195–4203.
44 M. Seredych, M. Khine and T. J. Bandosz, *ChemSusChem*, 2011, **4**, 139–147.
45 R. J. White, M. Antonietti and M. M. Titirici, *J. Mater. Chem.*, 2009, **19**, 8645–8650.
46 B. J. Lindberg, K. Hamrin, G. Johansson, U. Gelius, A. Fahlman, C. Nordling and K. Siegbahn, *Phys. Scr.*, 1970, **1**, 286–298.
47 J. Zhang, *PEM Fuel Cell Electrocatalysts and Catalyst Layers: Fundamentals and Applications*, Springer, 2008.
48 T.-P. Fellinger, F. Hasché, P. Strasser and M. Antonietti, submitted.
49 Y. Y. Shao, J. H. Sui, G. P. Yin and Y. Z. Gao, *Appl.Catal., B–Environ.*, 2008, **79**, 89–99.
50 Q. H. Yang, W. H. Xu, A. Tomita and T. Kyotani, *Chem. Mater.*, 2005, **17**, 2940–2945.
51 Z. Luo, S. Lim, Z. Tian, J. Shang, L. Lai, B. MacDonald, C. Fu, Z. Shen, T. Yu and J. Lin, *J. Mater. Chem.*, 2011, **21**, 8038–8044.
52 V. V. Strelko, V. S. Kuts and P. A. Thrower, *Carbon*, 2000, **38**, 1499–1503.
53 R. A. Sidik, A. B. Anderson, N. P. Subramanian, S. P. Kumaraguru and B. N. Popov, *J. Phys. Chem. B*, 2006, **110**, 1787–1793.
54 E. Chamorro, A. Toro-Labbe and P. Fuentealba, *J. Phys. Chem. A*, 2002, **106**, 3891–3898.
55 S. Scheiner and L. D. Bigham, *J. Chem. Phys.*, 1985, **82**, 3316–3321.